PNAS

Supplementary Information for

Mechanism of voltage sensing in Ca^{2+}- and voltage-activated K^+ (BK) channels

Willy Carrasquel-Ursulaez, Ignacio Segura, Ignacio Díaz-Franulic, Felipe Echeverría, Yenisleidy Lorenzo-Ceballos, Nicolás Espinoza, Maximiliano Rojas, Jose Antonio Garate, Eduardo Perozo, Osvaldo Alvarez, Fernando D. Gonzalez-Nilo, and Ramón Latorre.

Corresponding authors: Ramon Latorre or Fernando D. Gonzalez-Nilo
Email: ramon.latorre@uv.cl, or fernando.gonzalez@unab.cl.

This PDF file includes:

Supplementary Information Text

SI Appendix Materials and Methods

Channel expression. BK channels were expressed in *Xenopus laevis* oocytes. The cDNA coding for the wild-type human BK α-subunit (Gen bank U11058) was provided by L. Toro (University of California, Los Angeles, CA). All the mutants were prepared by standard molecular biology methods and confirmed by sequencing. The mRNA was prepared *in vitro* by using mMESSAGE mMACHINE (Ambion) kit. The oocytes were injected with 50 ng of mRNA and incubated in an ND96 solution (96 mM NaCl, 2 mM KCl, 1.8 mM $CaCl_2$, 1 mM $MgCl_2$, 5 mM HEPES, pH adjusted to 7.4 with NaOH) at 18°C for 4–8 days before electrophysiological recordings.

Electrophysiological recordings. All the recordings were acquired by using the patch-clamp technique in the inside-out configuration. Data were acquired with an Axopatch 200B (Molecular Devices) amplifier and the Clampex 10 (Molecular Devices) acquisition software. Both the voltage command and current output were filtered at 20 kHz with 8-pole Bessel low-pass filter (Frequency Devices). Current signals were sampled with a 16-bit A/D converter (Digidata 1550B; Molecular Devices), using a sampling rate of 500 kHz. Unless otherwise stated, linear membrane capacitance and leak subtraction were performed based on a P/-8 protocol (1) Borosilicate capillary glasses (1B150F-4, World Precision Instruments) were pulled in a horizontal pipette puller (Sutter Instruments). After fire-polishing, pipette resistance was typically 0.5-1 MΩ. An agar bridge with Na $MeSO_3$ as main anion was used as the ground electrode. All experiments were performed at room temperature (20-22 °C).

Gating currents (I_g) were elicited by 1-ms voltage steps of 10 mV, the holding and the voltage final values were chosen depending of the $Q(V)$ characteristics of each mutant: the holding voltage was -90 mV except for D186N, R207Q and R210Q mutants, for which holding voltages were -120 mV, 90 mV and 0 mV, respectively; the final voltage was 350 mV except for D153N (400 mV), R167Q (400 mV), D186N (300 mV), R207Q (-350 mV), R210Q (-400 mV) and R213Q (400 mV). The external (pipette) solution contained 110 mM tetraethylammonium (TEA), 10 mM HEPES, 2 mM HCl. The internal solutions (bath) contained 110 mM *N*-methyl-D-glucamine (NMDG), 10 mM HEPES, 2 mM HCl and 5 mM EGTA (free Ca^{2+} ~0.5 nM, based on the presence of ~10 μM contaminant [Ca^{2+}] (2)). For both solutions, the pH was adjusted to 7.4 with 108 mM methanosulfonic acid ($HMeSO_3$).

Potassium currents (I_K) were elicited by 10-ms voltage steps of 10 mV; the holding and the final voltage values were chosen depending of the $G(V)$ characteristics of each mutant: the holding voltage was -100 mV except for R207Q mutant, for which the holding voltage was -200 mV; the final voltage was 300 mV except for D153N (400 mV), R167Q (400 mV), D186N (300 mV), R210Q (-400 mV) and R213Q (400 mV). The pipette and bath solutions were the same and contained 110 mM KOH, 10 mM HEPES, 2 mM HCl, 1 mM EGTA (free Ca^{2+} ~0.5 nM), and the pH was adjusted to 7.4 with 108 mM $HMeSO_3$.

Proton currents (I_H) in mutant R210H were elicited by 10-ms and 3 ms voltage steps of -10 mV, the holding potential was 0 mV, and the final voltage was -400 mV. The pipette solution contained 110 mM TEA, 2 mM $MgCl_2$, 1 mM EGTA, and either 10 mM 2-(N-morpholino) methanesulfonic acid ($MeSO_3$) for solutions with final pH ≤5.5 or 10 mM HEPES for final pH >5.5. The bath solution contained 110 mM NMDG, 10 mM HEPES, 1 mM EGTA (free Ca^{2+} ~0.8 nM) and the pH was adjusted to 7.4 with 108 mM HMeSO3.

Data Analysis. For each experiment, the first 100 μs of the voltage-elicited gating currents (I_g) were fitted to a single exponential function and the area under the entire curve was integrated to obtain the charge displaced between closed states $Q_{c,i}(V)$, by using Clampfit 10 (Molecular Devices) and Matlab (MathWorks), as previously reported (3-5). $Q_{c,i}(V)$ data for each experiment i were fitted by using a Boltzmann function,

$$Q_{c,i}(V) = \frac{Q_{c,i,max}}{1 + e^{\left(\frac{-z_{Q,i}F(V-V_{0,i})}{RT}\right)}} \qquad [7]$$

where $Q_{c,i,max}$ is the maximum charge, $z_{Q,i}$ is the voltage dependency of voltage sensor activation, $V_{0,i}$ is the half-activation voltage, T is the absolute temperature (294 K), F is the Faraday's constant, and R is the universal gas constant. The best values for $Q_{c,i,max}$, $V_{0,i}$ and $z_{Q,i}$ were determined by using the Matlab lsqnonlin function. The averaged half-activation voltage ($\langle V_0 \rangle$) and the averaged voltage-dependency ($\langle z_Q \rangle$) were reported as mean ± S.E.M for the n experiments. Each individual $Q_{c,i}(V)$ curve was normalized by dividing by their specific $Q_{c,i,max}$ value and then aligned by shifting along the voltage axis by $(\langle V_0 \rangle - V_{0,i})$. A further shift of the $Q_{c,i}(V)$ curves was done by rounding each voltage value to the nearest ten. Finally, the values at each voltage were averaged and reported as mean ± S.E.M. This averaged $Q_c(V)$ relationship was fitted with a Boltzmann function (Eq. 8). This procedure generated an averaged curve with a voltage dependence representative of the n experiments (6).

$$Q_c(V) = \frac{1}{1 + e^{\left(\frac{-z_Q F(V - V_0)}{RT}\right)}} \qquad [8]$$

For ion and proton currents experiments, the instantaneous $I_{tail,i}(V)$ data for each i experiment were fitted by using a Boltzmann function,

$$I_{tail,i}(V) = \frac{I_{tail,i,max}}{1 + e^{\left(\frac{-z\delta_i F(V - V_{h,i})}{RT}\right)}} \qquad [9]$$

where $I_{tail,i,max}$ is the maximum tail current, $z\delta_i$ is the voltage dependency of activation of the channel, $V_{h,i}$ is the half-activation voltage, and T, F, and R are defined as described above. The best values for $I_{tail,i,max}$, $V_{h,i}$, and $z\delta_i$ were determined by using Matlab´s lsqnonlin function. The averaged half-activation voltage ($\langle V_h \rangle$) and the averaged voltage-dependency ($\langle z\delta \rangle$) were reported as mean ± S.E.M for the n experiments. Normalized $I_{tail,i}/I_{tail,i,max}$ curves were obtained by dividing $I_{tail,i}(V)$ curves by their specific $I_{tail,i,max}$ value and then aligned by shifting them along the voltage axis by $(\langle V_h \rangle - V_{h,i})$. A further shift of the $I_{tail,i}/I_{tail,i,max}$ curves was done by rounding each voltage value to the nearest ten. Finally, the values at each voltage were averaged and reported as mean ± S.E.M. This averaged $I_{tail}/I_{tail,max}$ relationship was fitted with a Boltzmann function for every construct. This procedure generated an averaged curve with a voltage dependence representative of the n experiments (6). The normalized curves obtained by doing this procedure were also fitted using Eq. 5 given in Results.

Molecular modeling

Solvation and Electrostatic profiles of the Voltage Sensor Domain. To initially explore the degree of hydration and the electrostatic maps of the BK VSD, we employed the 3.5 Å resolution Cryo-EM structure of hBK+β4 obtained from the Protein Data Bank (PDB), entry code 6V35 (7). Hydrogen and missing atoms were added using the internal coordinates of Charmm36 topology files (8, 9) assuming a pH of 7.0 for protonation states; the protonation state of all histidines was chosen as neutral. The model was built employing the VMDv1.93 (10) software, made up by the α-hBK homotetramer embedded in a preequilibrated and solvated palmitoyloleoylphosphatidyl-ethanolamine lipid bilayer placed in the x-y plane (11). Overlapping lipids were removed and a solvation shell was added in the z and -z direction; the z-axis was set as normal to the bilayer. The final system size was of 144x144x120 $Å^3$ with a total of around 250 K atoms. For a graphical depiction of the simulated system, refer to Fig. 2, *A* and *B*. MD simulations were performed with the NAMDv2.14 program (12), utilizing the CHARMM36 parameter set (13) and the TIP3P water model (14). Every production run was performed coupled to an isothermal-isobaric ensemble (NPT) reservoir (with constant cross sectional x-y surface) with set points of 1 atm and 298 K using the Nosé-Hoover method (15) and Langevin dynamics for piston fluctuation and temperature control with a damping coefficient of 1 ps^{-1} (16). The SHAKE algorithm was applied to constrain the lengths of all bonds involving water or hydrogen atoms (17). For full long-range electrostatics the Particle Mesh Ewald method (18) was used within a relative tolerance of $1x10^{-6}$. A cut-off distance of 12 Å was applied to real-space Ewald interactions. The same value was employed for the van der Waals interactions with a smooth switching function applied to within 10 and 12 Å. Prior to production simulations, an initial thermalization (2000 steps) followed by an NPT run. Equilibrium MD

simulations were then performed for 0.6 μs, with the first 0.1 μs considered as further relaxation. After the production run, the multiple protein conformations throughout the trajectory were clustered in terms of structural similarity via the K-means algorithm employing an RMSD (Cα) cut-off of 2.5 Å (19). From the centroid of the most populated clusters, the transmembrane domain (residues 93 to 326 of the α subunit) was further simulated (500 ns); from the representative structure of this production run, the R207Q and D153N mutants were prepared by replacing the side-chains of positions 207 or 153 by means of VMDvv1.93 (10). These systems were simulated using the same protocols mentioned above. Trajectory analysis was carried out by TCL scripting and VMD. This allowed us to determine mean relative water, R210 and R213 densities, and salt bridges presented within the VSD structure.
Due to the inherent protein flexibility, the representative structure for the wild type MD was further simulated keeping the protein fixed for 2 ns. Afterwards, average electrostatic potentials were computed by solving Poisson's equation in a grid via the PMEPot plugin of VMDv1.93 (20) with an Ewald factor of 0.5.
Activation of Voltage Sensor Domain and Gating Charges Movement. Small loops of the BK structure were completed and refined using the MODELLER package; loops were then subjected to a short relaxation using MD (21-23). Loops longer than 15 aa (residues 55-90, 616-680 and 834-870) were generated with QUARK (24, 25) server to generate a 3D structure (24). Its algorithm is based on a fragment-assembly method developed by the Yang Zhang Lab. Later, monomers were assembled with Multiseq tool in VMD using as a reference the 6V35 structure.

For the next step, the model was placed into a POPC (1-palmitoyl-2-oleoyl-phosphatidylcholine) membrane, composed of 685 lipids and surrounded by 112,503 water molecules and ions (1128 K^+, 1072 Cl^-), resulting in a salt concentration of 0.5 M. The dimensions of the final system are 194 x 187 x 179 $Å^3$. The system was relaxed by MD with the AMBER software package (26), starting from a protein structure restrained in the loops using a harmonic restraint of 10 kcal·mol^{-1}Å^{-2}. Restraints were then gradually released by applying smaller force constants (10, 5, 2.5, 1.0, 0.5, 0 kcal·mol^{-1} Å^{-2}). 500 ns of MD were completed with a timestep of 2 fs. van der Waals interactions were computed (14) using a cutoff of 1.0 nm, and the dispersion correction for energy and pressure was used. The particle mesh Ewald (PME) method was applied for electrostatic interactions (18). The Amber19SB force field was used for proteins (27), LIPID 17 force field for lipids (28), the TIP3P water model (14), and ion parameters reported by Joung and Cheatham (29). Temperature was kept constant using the velocity rescale (v-rescale) thermostat (30). The semi-isotropic Berendsen barostat (31) was used to keep the pressure at 1 atm, 310 K, and 1 bar.
After equilibration the system was subjected to an external electric field applied along the z-axis to generate the membrane voltage of 400 mV. The voltage (V) was calculated with:

$$V = ELz \qquad [10]$$

where E represents the applied electric field and Lz the length of the simulation box along the z-axis, as reported previously (32). A first run under electric field during ~3.9 μs and two replicas reaching ~2.3 μs were performed. Visual Molecular Dynamics (VMD) software (10) was used to build the system and generate images.

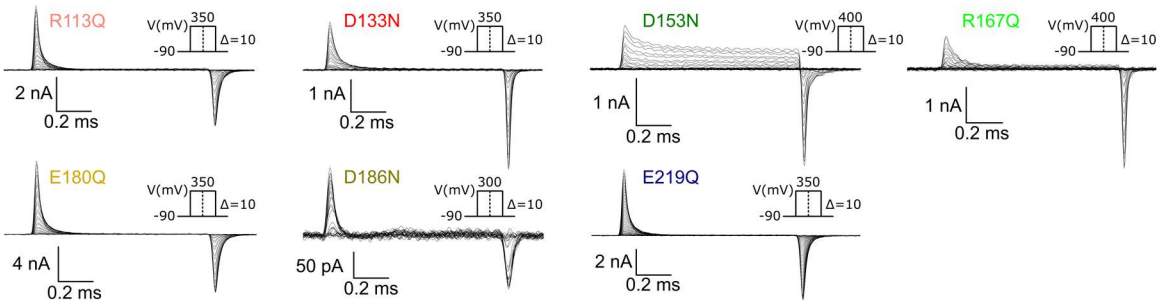

Fig. S1. Representative records of gating current of neutralization mutants R113Q, D133N, D153N, R167Q, E180Q, D186N, and E219Q.

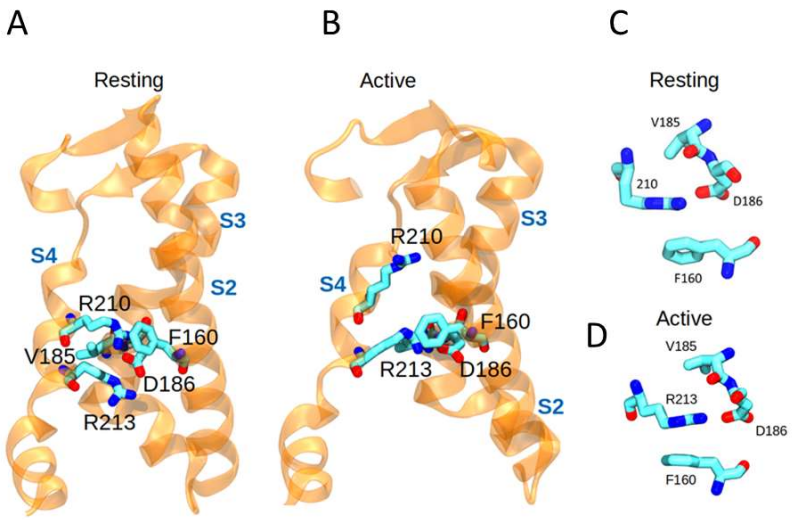

Fig. S2. (*A*) Transmembrane Segments S2, S3 and S4 in the BK VSD resting state. R210 is anchored to hydrophobic residues, F160 and V185, while forming a saline bridge with D186. (*B*) Transmembrane Segments S2, S3, and S4 in the BK VSD active state. When R210 moves up in response to the membrane electric field R213 is trapped by F160 and V185. Closer views of the residues surrounding R210 and R213 in the (*C*) resting and (*B*) active states. In both cases, the gating charges are stabilized by a π-cation interaction with F160.

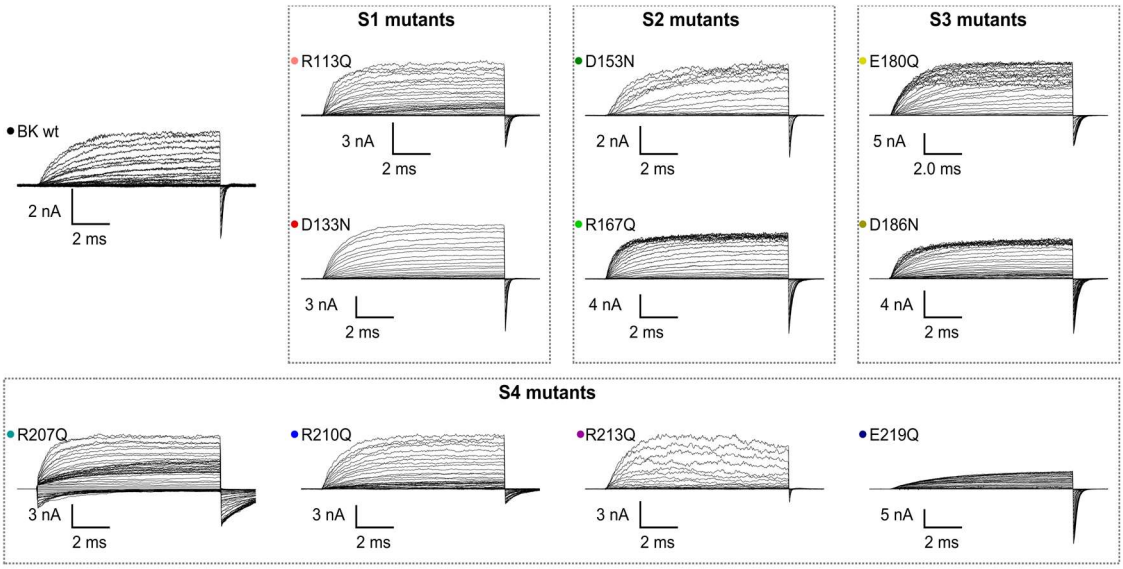

Fig. S3. Representative records of ionic current of wild type and neutralization mutants.

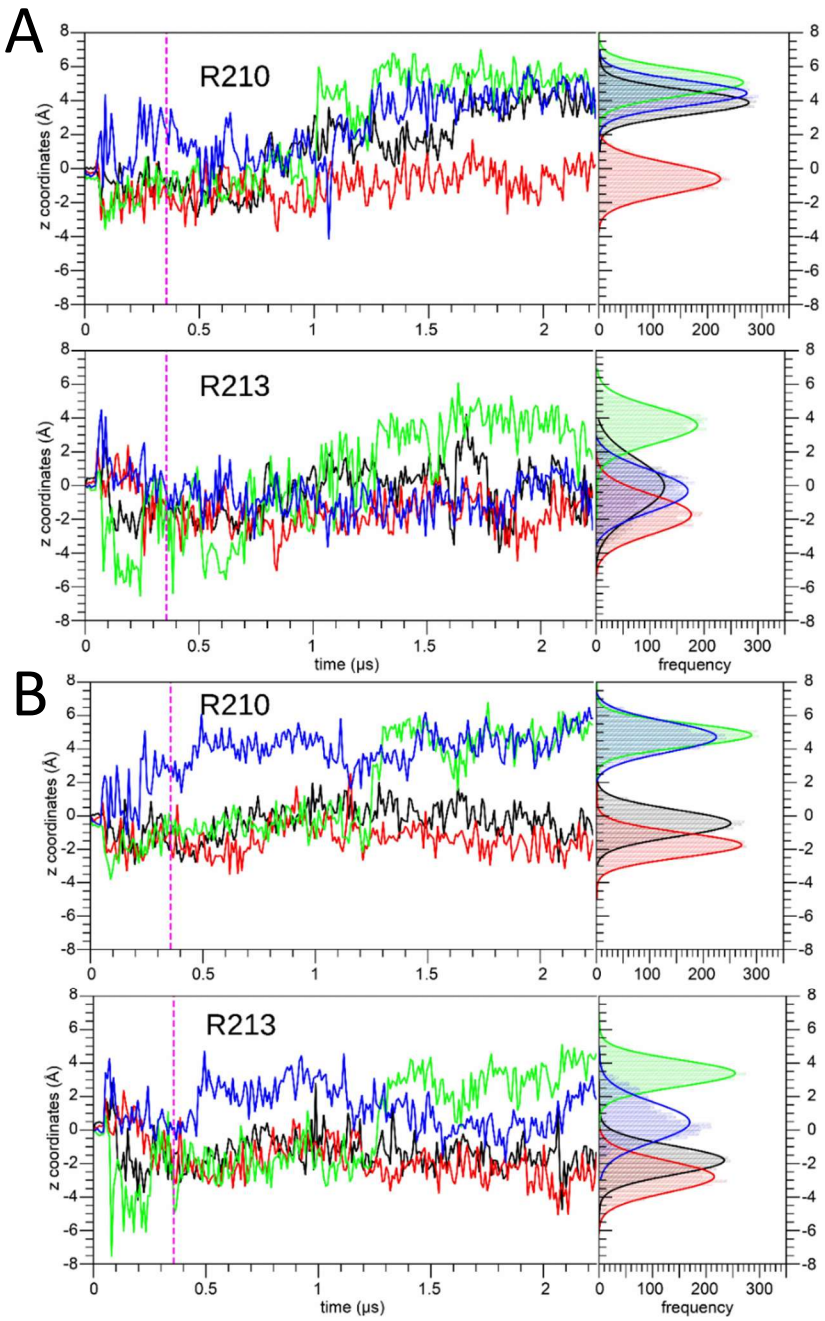

Fig. S4. Replicas of Molecular simulations shown in Fig. 5. (*A*) Replica #2. (*B*) Replica #3. Upper and lower panels show the z-axis displacement of the guanidine group CZ atom as a function of time for Arginine 210 and Arginine 213, respectively.

Table S1. Boltzmann fit parameters describing the activation of the voltage sensor domain of the BK channel.

Construct	V_0 (mV) (Mean ± SEM)	z_Q (Mean ± SEM)	N	$\Delta(\Delta G^0)$ (kJ)
WT	172 ± 3	0.62 ± 0.02	13	0.0
R113Q	170 ± 5	0.58 ± 0.01	8	-0.8
D133N	212 ± 3	0.59 ± 0.04	4	1.8
D153N	340 ± 7	0.65 ± 0.02	4	11.0
R167Q	289 ± 5	0.64 ± 0.01	5	7.6
E180Q	121 ± 8	0.55 ± 0.03	4	-3.9
D186N	72 ± 5	0.62 ± 0.03	11	-6.0
R207Q	-147 ± 3	0.63 ± 0.02	4	-19.2
R210Q	-342 ± 11	0.27 ± 0.02	6	-19.2
R210C	-370 ± 6	0.30 ± 0.01	3	-21.0
R210H	-366 ± 5	0.28 ± 0.02	5	-20.2
R210I	-350, -354	0.29, 0.30	2	-20.5
R210N	-361, -364	0.27, 0.28	2	-20.0
R213Q	394 ± 1	0.39 ± 0.01	3	4.5
R213H	402 ± 4	0.31 ± 0.01	22	1.7
R213C	398 ± 2	0.34 ± 0.02	13	2.8
E219Q	121 ± 6	0.59 ± 0.01	6	-3.4

V_0 is the voltage of half activation, z_Q is the voltage dependency of voltage sensor activation, $V_{0,i}$ is the half-activation voltage. N represents the number of experiments and $\Delta(\Delta G^0)$ is the Gibbs Free Energy difference between each mutant and wild-type channels.

Table S2. H-A model fit parameters of $G(V)$ curves for the wild type and neutralization mutants.

Construct	J_0	L_0 (Mean ± SEM)	z_L (Mean ± SEM)	D (Mean ± SEM)
WT	0.015	$1.03*10^{-6} \pm 4.02*10^{-8}$	0.34 ± 0.01	34.7 ± 0.86
R113Q	0.02	Equal to WT value	Equal to WT value	33.8 ± 0.09
D133N	0.0073	Equal to WT value	Equal to WT value	26.8 ± 0.29
D153N	0.00017	Equal to WT value	Equal to WT value	26.5 ± 1.29
R167Q	0.00069	Equal to WT value	Equal to WT value	22.6 ± 0.24
E180Q	0.072	Equal to WT value	Equal to WT value	21.4 ± 3.46
D186N	0.17	Equal to WT value	0.49 ± 0.01	10.8 ± 0.02
R207Q	25	Equal to WT value	0.42 ± 0.01	23.5 ± 0.26
R210Q	37	Equal to WT value	0.43 ± 0.01	11.9 ± 0.16
R213Q	0.0237	Equal to WT value	Equal to WT value	10.6 ± 0.12
E219Q	0.054	Equal to WT value	Equal to WT value	15.9 ± 0.83

J_0 represents the equilibrium constant for VSD activation at 0 mV, L_0 is the equilibrium constant for the Closed-Open transition at 0 mV, z_L is the voltage dependence of pore opening, and D is the allosteric coupling constant between the VSD and the pore domain. L_0 remained the same as that of the wild type for all mutants and z_L could vary for D186N, R207Q and R210Q to fit the data.

SI References

1. C. M. Armstrong, F. Bezanilla, Charge movement associated with the opening and closing of the activation gates of the Na channels. *J Gen Physiol* **63**, 533-552 (1974).
2. J. Cui, D. H. Cox, R. W. Aldrich, Intrinsic voltage dependence and Ca2+ regulation of mslo large conductance Ca-activated K+ channels. *J Gen Physiol* **109**, 647-673 (1997).
3. Y. Lorenzo-Ceballos, W. Carrasquel-Ursulaez, K. Castillo, O. Alvarez, R. Latorre, Calcium-driven regulation of voltage-sensing domains in BK channels. *Elife* **8** (2019).
4. W. Carrasquel-Ursulaez *et al.*, Hydrophobic interaction between contiguous residues in the S6 transmembrane segment acts as a stimuli integration node in the BK channel. *J Gen Physiol* **145**, 61-74 (2015).
5. G. F. Contreras, A. Neely, O. Alvarez, C. Gonzalez, R. Latorre, Modulation of BK channel voltage gating by different auxiliary beta subunits. *Proc Natl Acad Sci U S A* **109**, 18991-18996 (2012).
6. F. T. Horrigan, R. W. Aldrich, Coupling between voltage sensor activation, Ca2+ binding and channel opening in large conductance (BK) potassium channels. *J Gen Physiol* **120**, 267-305 (2002).
7. X. Tao, R. MacKinnon, Molecular structures of the human Slo1 K. *Elife* **8** (2019).
8. J. Huang *et al.*, CHARMM36m: an improved force field for folded and intrinsically disordered proteins. *Nat Methods* **14**, 71-73 (2017).
9. A. D. MacKerell, Jr., M. Feig, C. L. Brooks, 3rd, Improved treatment of the protein backbone in empirical force fields. *J Am Chem Soc* **126**, 698-699 (2004).
10. W. Humphrey, A. Dalke, K. Schulten, VMD: Visual molecular dynamics. *Journal of Molecular Graphics* **14**, 33-38 (1996).
11. J. B. Klauda *et al.*, Update of the CHARMM all-atom additive force field for lipids: validation on six lipid types. *J Phys Chem B* **114**, 7830-7843 (2010).
12. J. C. Phillips *et al.*, Scalable molecular dynamics with NAMD. *J Comput Chem* **26**, 1781-1802 (2005).
13. K. Vanommeslaeghe *et al.*, CHARMM general force field: A force field for drug-like molecules compatible with the CHARMM all-atom additive biological force fields. *J Comput Chem* **31**, 671-690 (2010).
14. W. L. Jorgensen, J. Chandrasekhar, J. D. Madura, R. W. Impey, M. L. Klein, Comparison of simple potential functions for simulating liquid water. *The Journal of Chemical Physics* **79**, 926-935 (1983).
15. G. J. Martyna, D. J. Tobias, M. L. Klein, Constant-Pressure Molecular-Dynamics Algorithms. *J Chem Phys* **101**, 4177-4189 (1994).
16. G. S. Grest, K. Kremer, Molecular-Dynamics Simulation for Polymers in the Presence of a Heat Bath. *Phys Rev A* **33**, 3628-3631 (1986).
17. J. P. Ryckaert, G. Ciccotti, H. J. C. Berendsen, Numerical-Integration of Cartesian Equations of Motion of a System with Constraints - Molecular-Dynamics of N-Alkanes. *J Comput Phys* **23**, 327-341 (1977).
18. T. Darden, D. York, L. Pedersen, Particle mesh Ewald: An N·log(N) method for Ewald sums in large systems. *The Journal of Chemical Physics* **98**, 10089-10092 (1993).
19. M. E. Karpen, D. J. Tobias, C. L. Brooks, Statistical Clustering-Techniques for the Analysis of Long Molecular-Dynamics Trajectories - Analysis of 2.2-Ns Trajectories of Ypgdv. *Biochemistry-Us* **32**, 412-420 (1993).
20. A. Aksimentiev, K. Schulten, Imaging alpha-hemolysin with molecular dynamics: ionic conductance, osmotic permeability, and the electrostatic potential map. *Biophys J* **88**, 3745-3761 (2005).
21. B. Webb, A. Sali, Comparative Protein Structure Modeling Using MODELLER. *Curr Protoc Bioinformatics* **54**, 5 6 1-5 6 37 (2016).
22. A. Sali, T. L. Blundell, Comparative protein modelling by satisfaction of spatial restraints. *J Mol Biol* **234**, 779-815 (1993).
23. A. Fiser, R. K. Do, A. Sali, Modeling of loops in protein structures. *Protein Sci* **9**, 1753-1773 (2000).
24. D. Xu, Y. Zhang, Ab initio protein structure assembly using continuous structure fragments and optimized knowledge-based force field. *Proteins* **80**, 1715-1735 (2012).

25. D. Xu, Y. Zhang, Toward optimal fragment generations for ab initio protein structure assembly. *Proteins* **81**, 229-239 (2013).
26. T. S. Lee *et al.*, Alchemical Binding Free Energy Calculations in AMBER20: Advances and Best Practices for Drug Discovery. *J Chem Inf Model* **60**, 5595-5623 (2020).
27. C. Tian *et al.*, ff19SB: Amino-Acid-Specific Protein Backbone Parameters Trained against Quantum Mechanics Energy Surfaces in Solution. *J Chem Theory Comput* **16**, 528-552 (2020).
28. C. J. Dickson *et al.*, Lipid14: The Amber Lipid Force Field. *J Chem Theory Comput* **10**, 865-879 (2014).
29. I. S. Joung, T. E. Cheatham, Determination of Alkali and Halide Monovalent Ion Parameters for Use in Explicitly Solvated Biomolecular Simulations. *The Journal of Physical Chemistry B* **112**, 9020-9041 (2008).
30. G. Bussi, D. Donadio, M. Parrinello, Canonical sampling through velocity rescaling. *The Journal of Chemical Physics* **126**, 014101 (2007).
31. H. J. C. Berendsen, J. P. M. Postma, W. F. v. Gunsteren, A. DiNola, J. R. Haak, Molecular dynamics with coupling to an external bath. *The Journal of Chemical Physics* **81**, 3684-3690 (1984).
32. B. Roux, The membrane potential and its representation by a constant electric field in computer simulations. *Biophys J* **95**, 4205-4216 (2008).